

Lignin-containing Nanocellulose for in situ Chemical-Free Synthesis of AgAu-based Nanoparticles with Potent Antibacterial Activities

Yisheng Sun, Qianwei Li, Xiangwei Du, Velaphi Thipe, Bongkosh Vardhanabhuti, Shramik Sengupta, Kattesh Katti, and Caixia Wan*



Cite This: *ACS Omega* 2022, 7, 41548–41558



Read Online

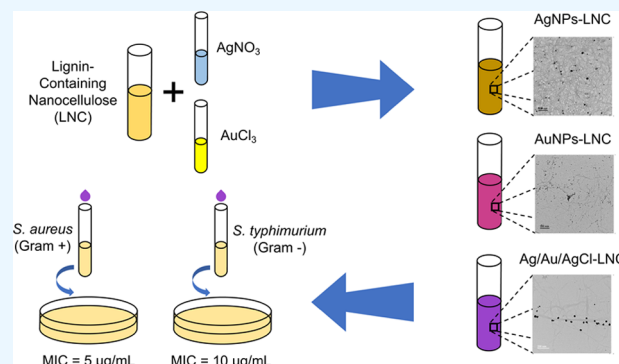
ACCESS |

Metrics & More

Article Recommendations

Supporting Information

ABSTRACT: Lignin-containing nanocelluloses (LNCs) have the properties of both lignin and nanocellulose and could overcome the limits of both individual components in metallic nanoparticle synthesis. However, studies on LNCs are still limited, and the potential of such nanomaterials for metallic nanoparticle synthesis has not been fully unraveled. In this study, monometallic silver, gold nanoparticles, and Ag–Au–AgCl nanohybrids were synthesized in situ utilizing LNCs in a chemical-free approach. The parameters, including Ag^+ and Au^{3+} concentrations as well as $[\text{Au}^{3+}]/[\text{Ag}^+]$ ratios, were investigated for their effects on the nanoparticle synthesis. The characterizations, including UV–vis spectrophotometry, transmission electron microscopy (TEM), X-ray photoelectron spectroscopy (XPS), X-ray powder diffraction (XRD), and Fourier transform infrared spectroscopy (FTIR), confirmed the coexistence of Ag, Au, and AgCl while indicating the key role of lignin and oxygen-containing functional groups in the nanoparticle synthesis. The as-synthesized AgNPs-, AuNPs-, and nanohybrids-LNC samples were tested for their antibacterial activities. In comparison to the monometallic AgNPs-LNC sample, nanohybrids-LNC synthesized with 0.063 mM Au^{3+} loading showed superior antibacterial activities with minimum inhibitory concentrations (MICs) at 5 $\mu\text{g}/\text{mL}$ against Gram-positive *Staphylococcus aureus* and 10 $\mu\text{g}/\text{mL}$ against Gram-negative *Salmonella typhimurium* with controlled Ag^+ release. The results indicated that LNCs can be used to synthesize metallic nanoparticles, and the resultant Ag–Au–AgCl nanohybrids were a potent antibacterial agent with reduced environmental impacts.



1. INTRODUCTION

Infectious diseases and antimicrobial resistance are becoming a more and more urgent threat to public health worldwide.¹ To fight against this threat, tremendous efforts have been devoted to developing novel antimicrobial materials, among which metallic nanoparticles are an important family.² Across metallic nanoparticles, AgNPs are well known for their broad-spectrum antimicrobial activities, making them a viable class of agents for combating multidrug-resistant pathogens.³ The antimicrobial efficacy of AgNPs is ascribed to reactive oxygen species (ROS) generated by Ag^+ ions released from AgNPs, which causes damage of cell membranes and interference with metabolic components such as DNA and proteins.³ In recent years, an increasing body of research asserted that nanocomposites of AgNPs with coexisting nanomaterials could enhance their antimicrobial activities while mitigating their negative environmental impacts and cytotoxicity caused by the discharge of Ag^+ ions.^{4–6} Bimetallic gold–silver nanoparticles (Au–AgNPs) exhibit superior antimicrobial properties with reduced silver loadings compared to monometallic AgNPs, likely due to activation of surface silver atoms by gold.^{7,8} Nudelman and co-workers also reported the photothermal properties of

bimetallic Au–Ag nanoparticles under near-IR light, which successfully removed biofilms of *Bacillus subtilis*.⁹ In addition, Au–AgNPs tend to possess lower cytotoxicity and better biocompatibility than AgNPs,^{10,11} which could be attributed to a controlled release of Ag^+ ions. Non-noble metal also exhibited synergistic properties with Ag, e.g., bimetallic Ag–Fe nanoparticles, in antimicrobial applications against multi-drug-resistant pathogens.¹² Similarly, Ag–AgCl nanohybrids were found to be a less toxic alternative to AgNPs while retaining a strong antimicrobial efficacy.^{13–16} Moreover, the unique properties of the Ag–AgCl nanohybrids make them more versatile than their individual counterparts in applications such as photocatalysis.^{17,18}

Polymeric materials are vastly involved in metallic nanoparticle synthesis and applications, exhibiting various functions

Received: August 22, 2022

Accepted: October 11, 2022

Published: October 31, 2022



such as stimulating and modulating nanoparticle formation as well as nanoparticle delivery and functionalization.¹⁹ As the most abundant polymers on Earth, cellulose and lignin have been investigated for metallic nanoparticle synthesis, particularly based on their nanoscale particles, i.e., nanocellulose and nanolignin. Nanocellulose and nanolignin are mainly produced from fractionation and disintegration of lignocellulosic biomass, both seen as substitutes for petroleum-based polymers and massively studied as multifunctional nanomaterials in the past decade.^{20–22} They both exhibit properties such as high porosity, large surface area, and good dispersibility, which make them potential capping agents for metallic nanoparticle synthesis.^{23,24} The distinctive aromatic nature of lignin specifically makes it capable of absorbing heavy metals such as Ag⁺ ions in an aqueous environment.^{25,26} Apart from their capping properties, nanocellulose and nanolignin can initiate the nucleation of heavy metal ions via reduction reactions.^{27,28} Functional groups in nanocellulose/nanolignin, such as –COOH,²⁹ –CHO,³⁰ and phenolic groups,³¹ are considered the sources of their reducing power, hypothetically making both materials potential for in situ synthesis of metallic nanoparticles without the use of other chemicals. However, most studies of nanocellulose and nanolignin in metallic nanoparticle synthesis by far still have limitations in that they require other chemicals,^{32,33} extra energy input,^{34,35} or surface functionalization^{30,36} to gain extra reducing powers needed for nanoparticle synthesis. Moreover, nanolignin preparation relies on certain solvent systems, such as alkaline solutions³⁷ and organic solvents,³⁸ which could pose extra barriers for the green synthesis of metallic nanoparticles. Particularly, synthesis of nanohybrids of more than one metallic compound using nanocellulose/nanolignin is found in a limited number of cases by far. A few examples were Au–AgNPs synthesized by cellulose,³⁹ Au–AgNPs synthesized by lignin,³⁷ and Ag–AgCl nanohybrids synthesized by cellulose,⁴⁵ all using alkaline solvents to dissolve cellulose or lignin.

In recent years, an emerging family of nanocellulose, lignin-containing nanocelluloses (LNCs), have sparked extensive research on its production, properties, and applications. In comparison to pure nanocellulose (cellulose only), LNC production does not entail the complete removal of lignin or extra processing for lignin nanofabrication and thus can reduce process complexity and lower production costs.⁴⁰ In terms of functions, LNCs, which combine the properties of nanocellulose and nanolignin, could have better potential than the two individual components and overcome their limitations in the green synthesis of metallic nanoparticles. LNCs, with excellent stability in pure aqueous dispersions, are suitable for chemical-free synthesis of metallic nanoparticles, and their unique surface chemistry due to the existence of lignin could potentially endow themselves with higher reducing powers than individual nanocellulose and nanolignin. Moreover, compared to nanolignin, LNCs are excellent natural building blocks due to nanocellulose as the backbone and could be easily fabricated into coatings,⁴¹ films,³² gels,⁴² and so forth to serve various application purposes. With coexisting lignin, LNCs can also provide add-on properties, such as hydrophobicity, UV-blocking, antioxidant capabilities, to the composite materials.^{43,44} By far, syntheses of metallic nanoparticles and nanohybrids using LNCs are still limited. In 2015, Hu and Hsieh successfully obtained monometallic AgNPs using lignin-coated cellulose clothes by mere boiling in pure water with no use of other chemicals.⁴⁵ Compared to

macroscale cellulose materials, nano-sized LNCs could potentially improve the synthesis efficiency and application performances due to their large surface areas.

In this study, based on the hypothesis that LNCs combine the properties of both cellulose and lignin and thus could possess great potential for the synthesis of metallic nanoparticles and nanohybrids, an in situ chemical-free reaction route in pure water with no extra energy input was specifically designed to synthesize monometallic AgNPs, AuNPs, and nanohybrids Ag–Au–AgCl. Parameters such as the concentrations and mixing ratios of Ag⁺ and Au³⁺ precursors were evaluated to understand the synthesis kinetics, and the surface chemistry of LNCs was also investigated to illustrate the reaction mechanism. As-synthesized nanoparticles and nanohybrids were characterized in terms of UV–vis absorbance, microscopic morphology, and elemental compositions to understand their properties. Finally, the nanoparticles- and nanohybrids-LNCs were tested for antibacterial activity against both Gram-positive and Gram-negative pathogens to evaluate the potential of such green-synthesized nanomaterials in real-world applications.^{46,47}

2. MATERIALS AND METHODS

2.1. Materials. Switchgrass was collected from the South Farm at the University of Missouri in Columbia, Missouri, USA. It was air-dried, ground through a 2 mm screen, and stored in an airtight container prior to use. 2,2,6,6-Tetramethylpiperidine-1-oxyl (TEMPO) radical, sodium bromide (ACS grade), sodium hypochlorite (11–15% chlorine), and gold chloride (≥64.4% Au) were purchased from Fisher. Silver nitrate solution (0.1 N) was purchased from Sigma-Aldrich.

2.2. Ag–Au–AgCl Nanohybrid Synthesis. LNCs (56.0 wt % cellulose and 27.2 wt % lignin, data not shown) were prepared by chemical nanofibrillation of lignin-containing pulp, as detailed in the [Supporting Information](#). Ag–Au–AgCl nanohybrids were facilely synthesized by a simple mixing-staying method. Briefly, LNC suspension (0.1 wt % consistency) was mixed with an equal volume of AgNO₃ (5 mM), AuCl₃ (1, 3, or 5 mM), or their mixtures in varied mixing ratios, as summarized in [Table S1](#). The mixture was kept static at room temperature for 24 h. Subsequently, the reaction mixtures were thoroughly washed by dialysis (12 000–14 000 Dalton) in deionized (DI) water for 30 min to remove unreacted ions. A LNC-free AgNP sample was synthesized by sodium borohydride⁴⁸ and utilized as a positive control in the antibacterial assay. Briefly, 5 mL of 2.3 mM AgNO₃ solution was dropwise mixed with 30 mL of 10 mM NaBH₄ under vigorous stirring in an Erlenmeyer flask in an ice water bath. The synthesis was terminated by removing the flask from the ice water bath once the color of the solution became stable. Unless otherwise specified, freshly synthesized nanocomposite suspensions were characterized and evaluated for antibacterial activities.

2.3. Antibacterial Assay. Bacterial species of both Gram-positive and Gram-negative, i.e., *Staphylococcus aureus* and *Salmonella typhimurium*, respectively, were used as the model strains to evaluate the antibacterial activities of monometallic AgNPs-, AuNPs-, and nanohybrids-LNC samples. First, the bacterial cells were inoculated from glycerol stock maintained at –20 °C into liquid Luria–Bertani (LB) media and incubated at 37 °C overnight. Thereafter, the cells were collected by 3000g centrifugation for 5 min and resuspended in

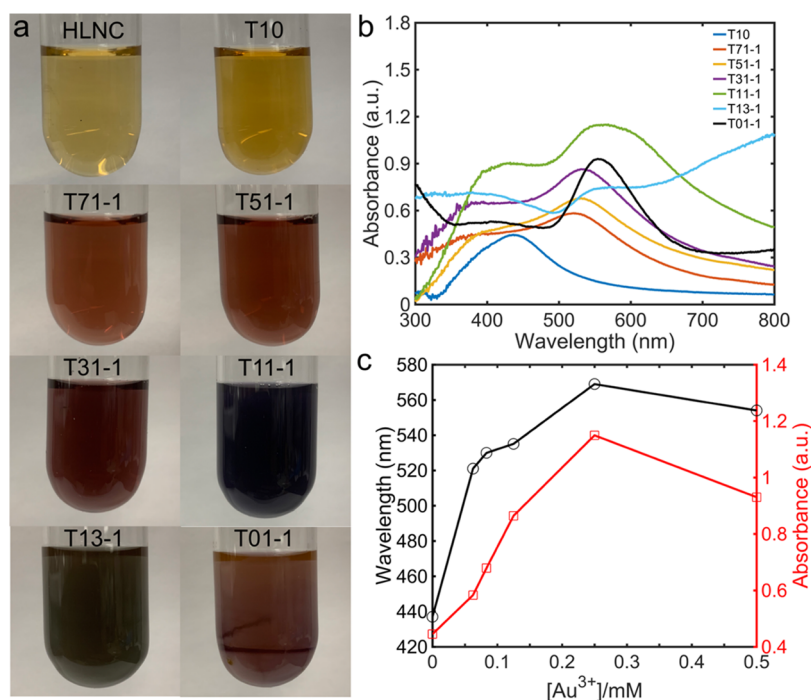


Figure 1. Synthesis of monometallic nanoparticles and nano hybrids by LNC. (a) Photos, (b) UV-vis spectra, and (c) peak wavelengths and absorbances of pristine LNC, and nanoparticles- and nano hybrids-LNC samples.

PBS buffer (pH 7.4). Subsequently, the cell suspension was transferred to LB media (diluted 5-fold by water) to reach a final cell concentration of 10^5 – 10^6 CFU/mL. T10, T71-1, T11-1, T01-1, or pristine LNC was then mixed with the cell suspension at a final concentration of 2, 5, or 10 μ g/mL, with sterile DI water as a negative control. The cell cultures were incubated at 37 °C with 500 rpm for 18 h and then diluted by 10^6 -fold with PBS buffer and spread onto LB agar plates, followed by static cultivation at 37 °C for 24 h. Finally, the CFUs on the agar cultures were counted. The antibacterial efficacies were determined by the reduction of CFUs over the negative control using sterile DI water. The results were statistically analyzed using a one-factor analysis of variance (ANOVA), with at least four replicates for each antimicrobial assay.

2.4. Characterization. The compositions of LNC were determined following a two-stage acid hydrolysis as described in the NREL protocol.⁴⁹ The ζ -potential of LNC was characterized by a Malvern Zetasizer (Malvern Instruments Ltd., GB). The LNC suspension was first diluted to a consistency of 0.02 wt % and then loaded in customized cells and scanned, setting water as the dispersant and the refractive index of LNC as 1.61.⁵⁰ UV-vis spectra of the metallic nanoparticles- and nano hybrids-LNC were obtained using a Cary 50 spectrophotometer (Varian, CA). The scanning was conducted from 200 to 800 nm at a middle speed with a background of pristine LNC suspension at a 0.05 wt % consistency. X-ray powder diffraction (XRD) was conducted with a Bruker SMART CCD system. Air-dried and pulverized samples were scanned at 0.02° /step from 20 to 70° . High-resolution transmission electron microscopy (HR-TEM) imaging was performed using both a JEOL JEM-1400 TEM and an FEI Tecnai F30 TEM equipped with an Oxford ultrathin window energy-dispersive X-ray (EDX) spectroscopy detector, running at 200 kV. Cell morphology was imaged with a JEOL JEM-1400 TEM. Bacterial cells of 10^6 – 10^7 CFU/mL

were treated with 10 μ g/mL nano hybrids-LNC sample (T71-1) in PBS buffer (pH 7.4) with an agitation rate of 500 rpm at 37 °C for 30 min. The cells were then collected via centrifugation at 14 000 rpm for 30 s and resuspended in 2% glutaraldehyde fixative for at least 30 min at room temperature for cell fixation. Silver ion release was analyzed by a Thermo Scientific iCAP 7000 Plus Series inductively coupled plasma-optical emission spectrometry (ICP-OES). Silver was detected at 243.78 nm with a linear calibration range from 0.1 to 100 μ g/mL. In the release test, AgNPs- or nano hybrids-LNC samples were added to 10 μ g/mL in 12 mL of diluted LB media and agitated at 500 rpm. Samples were collected at 0, 1, 2, 6, and 12 h, and then centrifuged at 12 000g for 10 min to remove silver particles while retaining Ag^+ ions. X-ray photoelectron spectroscopy (XPS) was conducted with a Thermo Scientific Nexsa PS system using a true monochromatic Al $K\alpha$ X-ray source (72 W, 400 μ m slot). Whole-spectrum survey (0.50 eV/step, dwell time 50 ms, pass energy 200 eV) and high-resolution scans (0.10 eV/step, dwell time 50 ms, pass energy 50 eV) of specific elements (C, O, Cl, Ag, Au) were both acquired. XPS spectra were analyzed with CasaXPS software and peak fitting was based on the Gaussian-Lorentzian line shape and Shirley background. Fourier transform infrared spectroscopy (FTIR) was conducted using a Nicolet 4700 FTIR spectrometer (Thermo Electron Corp., Waltham, MA) in attenuated total reflectance (ATR) mode equipped with a germanium crystal surface. All samples were scanned at 4 cm^{-1} per step through 400 to 4000 cm^{-1} wavenumbers.

3. RESULTS AND DISCUSSION

3.1. Synthesis of Ag–Au–AgCl Nano hybrids. The successful synthesis of metallic nanoparticles and nano hybrids was first identified by the color change of the LNC suspensions (Figure 1a). After 24 h, the monometallic AgNPs and AuNPs

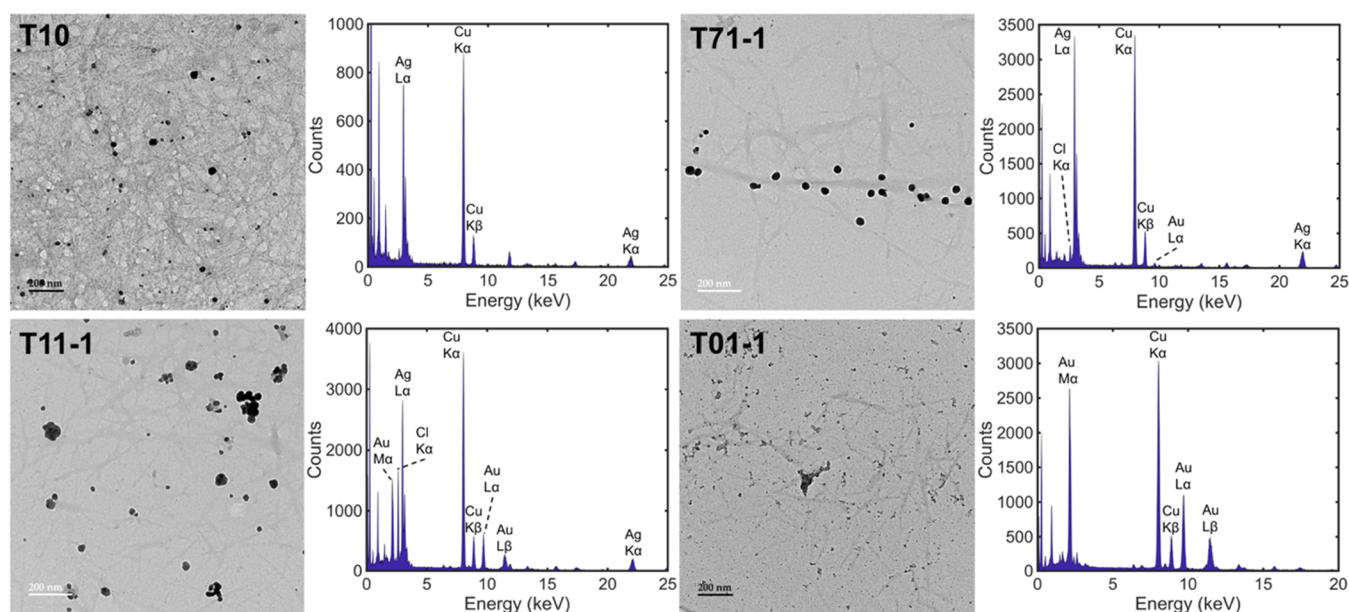


Figure 2. TEM images and EDS spectra of monometallic AgNPs- (T10), AuNPs- (T01-1), and nanohybrids-LNC (T71-1 and T11-1). T71-1 and T11-1 were synthesized by 0.029:1 and 0.20:1 molar ratio of $[\text{Au}^{3+}]/[\text{Ag}^+]$, respectively.

samples, T10 and T01-1, turned tawny and wine red, respectively, from the original light-tawny color of pristine LNC suspension. T01-1 also became slightly opaque and precipitates on the glass tube wall were observed, indicating potential aggregation of nanoparticles. In the nanohybrids-LNC samples, color changed differently when the ratios of precursors, i.e., AgNO_3 and AuCl_3 , varied. Across the samples with lower $[\text{Au}^{3+}]/[\text{Ag}^+]$ ratios, T71-1, T51-1, and T31-1, the colors were predominantly wine red but became darker as the $[\text{Au}^{3+}]/[\text{Ag}^+]$ ratio increased. When the ratio increased, the colors of T11-1 and T13-1 became dark blue and dark green, respectively. Characteristic light absorbance of the samples was measured using UV–vis spectroscopy, as illustrated in Figure 1b. It is well established that the effect of localized surface plasmon resonance leads to the special colors of noble metal particles when their size drops down to nanoscale, in which their dipolar electromagnetic fields formed by oscillating surface electrons were highly enhanced, and therefore, light of similar frequency to the oscillating surface electrons will be strongly absorbed and scattered, leaving a characteristic peak on the spectrum.⁵¹ The characteristic peaks of spherical AgNPs and AuNPs are typically around 400–440⁵² and 520–530 nm,⁵³ respectively, but may vary depending on size, shape, and surrounding environment. In Figure 1b, characteristic absorbance peaks of the monometallic samples, T10 (AgNPs-LNC) and T01-1 (AuNPs-LNC), were observed at 437 and 554 nm, respectively, indicating that AgNPs and AuNPs were successfully synthesized by LNC. The peak of T01-1 slightly red-shifted, and its absorbance of far-red lights (700–800 nm) became stronger, potentially due to size growth of AuNPs and the LNC aggregation being observed (Figure 1a).^{54,55} Since the LNC particles possessed negative surface charges (ζ -potential = -41.94 mV, data not shown), the results indicated that trivalent Au^{3+} ions might induce LNC aggregation more easily than monovalent Ag^+ ions at a lower concentration. In the nanohybrids-LNC samples, absorbance plateaus rather than single peaks were observed from around 400 to 560–600 nm, which varied depending on $[\text{Au}^{3+}]/[\text{Ag}^+]$ ratios. A previous study by Shin and colleagues reported the

absorbance peak of Au–Ag nanoalloys shifted from 395 to 525 nm as the molar fraction of Au increased from 0 to 1.¹⁰ A similar trend was observed when extracting the maximum absorbance over $[\text{Au}^{3+}]/[\text{Ag}^+]$ ratios (Figure 1c). Therefore, the absorbance plateaus were most likely caused by the coexistence of AgNPs, AuNPs, and Ag–Au alloys in distinct compositions. On the other hand, as Cl^- ions in AuCl_3 can combine with Ag^+ ions to generate AgCl , i.e., $\text{Ag}^+ + \text{Cl}^- \rightarrow \text{AgCl}$, AgCl could also pose an effect on the UV–vis absorbance. When existing individually, AgCl does not exhibit characteristic absorbance peaks, nor does exhibit significant absorbance of visible light (400–800 nm).^{56,57} However, the Ag/AgCl nanocomposite showed an overall enhanced absorbance plateau over UV and visible light spectra.^{56–58} This increased absorbance was most likely attributed to enhanced surface plasmon resonance of AgNPs when deposited on the surface of AgCl . As shown in Figure 1b, sample T13-1 exhibited an absorbance plateau between 200 and 800 nm with no distinguishable peaks, implying a dominant AgCl formation. Such absorbance-enhancing effect should also exist in the other nanohybrids-LNC samples, albeit at varying levels depending on the concentrations of Ag^+ , Au^{3+} , and Cl^- in synthesis, as described in the latter section. To better understand the role of lignin in the synthesis of nanoparticles, reactions utilizing bleached nanocellulose (BNC) (98.48 wt % cellulose and <1 wt % lignin) with similar $[\text{Au}^{3+}]/[\text{Ag}^+]$ ratios were conducted (Figure S1a and Table S2). After 24 h reaction, all the samples exhibited no absorbance peaks except strong absorbances between 200 and 300 nm, which were most likely caused by unreacted AgNO_3 and AuCl_3 (Figure S1b). Although AgCl might form without concurrent synthesis of metallic nanoparticles, AgCl alone could not cause light absorbance as discussed above.^{56,57} The results demonstrated that nanocellulose alone could not serve as a powerful reducing and capping agent to reduce Ag^+ and Au^{3+} ions under the given condition, underscoring the critical role of lignin in metallic nanoparticles synthesis. When using lignin-free nanocellulose to synthesize metallic nanoparticles,

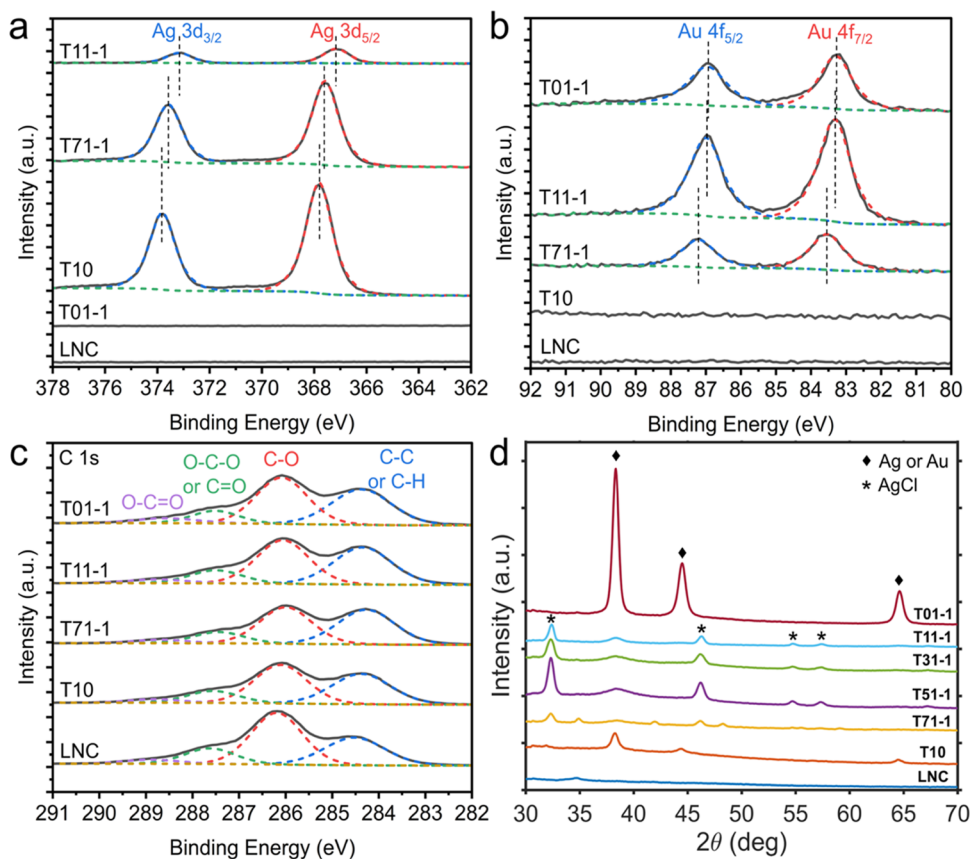


Figure 3. High-resolution XPS spectra of (a) Ag 3d, (b) Au 4f, and (c) C 1s regions, and (d) XRD patterns of pristine LNC, monometallic AgNPs-LNC (T10), AuNPs-LNC (T01-1), and nanohybrids-LNCs.

surface modifications^{23,30} and heated reactions^{28,29} are usually necessary.

The morphology and elemental composition of two monometallic samples, T10 and T01-1, together with two nanohybrids-LNC samples, T71-1 and T11-1, were determined using TEM equipped with an EDX detector (Figure 2). Throughout all the four samples, nanoparticles were observed adhering to the network structures formed by LNC. In nanohybrid T71-1 and T11-1, the metallic nanoparticles looked bigger in size, while aggregates were more frequently found in T11-1, which was likely attributed to the formation of AgCl and coexistence of different types of nanoparticles. Previous studies asserted that initially formed nanoparticles could induce the absorption of positively charged metal ions, such as Ag^+ and Au^{3+} , onto their surfaces, thereby facilitating the synthesis of nanoparticles.^{59,60} In the EDX spectra, the Cl signal was only detected in the spectra of nanohybrids-LNC samples, implying that it existed in AgCl. Comparing T71-1 and T11-1, the Cl signal was greater in T11-1, indicating that AgCl formation was promoted under conditions of increased $[\text{Au}^{3+}]/[\text{Ag}^+]$ ratios.

3.2. Understanding the Mechanism of Nanohybrid Synthesis. To better understand the mechanism of nanoparticles synthesis by LNCs, the samples synthesized with different $[\text{Au}^{3+}]/[\text{Ag}^+]$ ratios were characterized by XPS (Figures 3a–c and S2 and Table S3). In the whole-range surveys, the characteristic O 1s and C 1s peaks were found across all the samples including the pristine LNCs, while the peaks of Ag, Au, and Cl were also observed in specific nanoparticles- and nanohybrids-LNC samples. The character-

istic Ag 3d peaks were detected in T10, T71-1, and T11-1 but not in the monometallic AuNPs-LNC sample, T01-1. In monometallic T10, Ag 3d_{3/2} and Ag 3d_{5/2} peaks were found at 373.81 and 367.81 eV, respectively, matching well with the binding energy of Ag^0 .⁶¹ Silver oxides, namely, Ag_2O and AgO , are common impurities in AgNPs synthesis, which lead to slight negative shifts of the Ag 3d peaks and could be difficult to distinguish from Ag^0 merely based on Ag spectra.⁶¹ Therefore, the O 1s spectra were concurrently inspected to distinguish Ag^0 versus silver oxides, as silver oxides show peaks between 529.2 and 528.4 eV. However, the signals within that region were almost negligible through all the samples analyzed (Figure S2c), indicating that the formation of Ag_2O and AgO was insignificant. In addition, in Ag nucleation, when AuCl_3 was added, the Ag 3d_{3/2} and Ag 3d_{5/2} peaks shifted to 373.58 and 367.58 eV in T71-1, and 373.16 and 367.15 eV in T11-1, respectively, showing a negative shift as the ratio of $[\text{Cl}^-]/[\text{Ag}^+]$ increased. Such correlation indicated that the formation of AgCl could be the cause of XPS peak shifts, which was also supported by prior studies.^{17,62} Ag–Au alloy could also cause similar peak shifts of Ag, while positively shifting Au 4f peaks.⁶³ In Figure 3b, compared to monometallic T01-1, the characteristic Au 4f_{7/2} peaks of T11-1 and T71-1 shifted by +0.03 and +0.25 eV, respectively, which suggested the formation of Ag–Au alloy. Following the order of T01-1, T11-1, and T71-1, the $[\text{Au}^{3+}]/[\text{Ag}^+]$ ratio decreased, which implied that the formation of Ag–Au alloy was enhanced when Ag^+ was in exceeding quantity, likely because Ag^+ preferentially bonded with Cl^- . The state of Cl was also inspected to confirm the formation of AgCl. In nanohybrid T71-1 and T11-1, Cl 2p_{3/2}

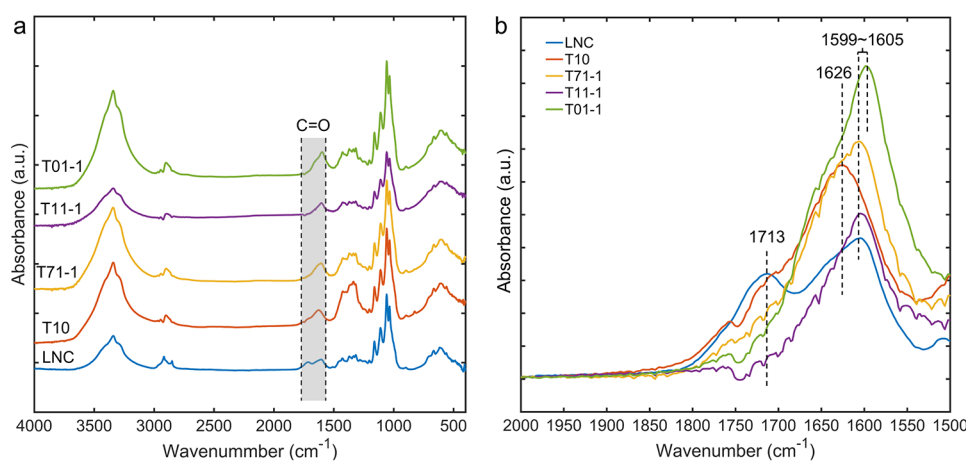


Figure 4. FTIR spectra, (a) whole-range and (b) C=O range with overlaid baselines of pristine LNC, monometallic AgNPs-LNC (T10), AuNPs-LNC (T01-1), and nanohybrids-LNCs (T71-1 and T11-1).

and $2p_{1/2}$ peaks were found around 197.4 and 199.1 eV, respectively, consistent with the reported binding energy in metal chlorides.^{17,64} In monometallic T01-1, Cl 2p peaks were found at the same positions, which might be attributed to residual AuCl_3 or Cl^- ions attached on the surface of AuNPs. Moreover, an extra minor peak was found at 201.59 eV in T01-1, likely assigned to organic chloride compounds,⁶⁴ which could be attributed to side reactions between AuCl_3 and LNCs when no Ag^+ existed. In the C 1s spectra, four peaks were deconvoluted at approximately 284.4, 286.1, 287.5, and 288.7 eV, assigned to carbon atoms in C–C/C–H, C–O, O–C–O/C=O, and O–C=O bonding, respectively, and no obvious differences in position were found through all the samples. Compared to pristine LNCs, the peak concentration of C–C/H increased from 31.32% to around 40% in all the nanoparticles- and nanohybrids-LNC samples (T01-1, T11-1, T71-1, T10), while their C–O concentrations decreased from 49.61 to 40.84–44.05% and O–C–O and C=O concentrations decreased from 14.75 to 10.92–13.33%. Such concentration changes inferred that the reduction of Ag^+ and Au^{3+} potentially involved oxygen-containing functional groups such as hydroxyl and aldehyde groups on LNCs. Meanwhile, the concentrations of carboxyl (O–C=O) groups remained relatively constant before and after the syntheses. XRD was also utilized to identify the crystal structures of Ag and Au nanoparticles and nanohybrids (Figure 3d). In T10 and T01-1, characteristic Bragg reflection peaks of mere Ag^0 and Au^0 were found, whereas AgCl peaks appeared along with those of silver or gold in all nanohybrids-LNC samples, indicating the coexistence of Ag^0 , Au^0 , and AgCl.^{65,66}

FTIR could also detect the changes in functional groups of LNCs after nanoparticles synthesis. In Figure 4, absorbance changes were found within the region of C=O stretching which was likely related with carboxyl groups in LNCs. After overlaying the spectra on the same baseline (Figure 4b), absorbance peaks at 1713 and 1605 cm^{-1} were found in pristine LNC corresponding to acidic COOH and carboxylate salts (COO^-). The absorbance at 1713 cm^{-1} almost completely disappeared in all the other samples after nanoparticles synthesis. Considering that the carboxyl (O–C=O) groups were not consumed based on XPS spectra, their absorbance peaks on FTIR spectra could shift to other locations within the region due to different binding states.⁶⁷ In monometallic T10, the peak at 1605 cm^{-1} also disappeared

while a major absorbance was observed at 1626 cm^{-1} , which might be attributed to the interaction between carboxyl groups and AgNPs.⁶⁸ In T01-1, the main absorbance was observed at 1599 cm^{-1} , which did not shift noticeably from 1605 cm^{-1} in pristine LNC and indicated that AuNPs did not strongly interact with carboxyl groups. In nanohybrid T71-1 and T11-1, the major absorbance peaks appeared at 1605 cm^{-1} , shifted from 1626 cm^{-1} in T10, suggesting removal of the interactions between AgNPs and carboxyl groups.

The synthesis kinetics of Ag–Au–AgCl nanohybrids were investigated with various Au^{3+} concentrations and $[\text{Au}^{3+}]/[\text{Ag}^+]$ ratios over the course of 24 h reaction. Figure S3 shows the UV–vis spectra of the nanohybrids-LNC samples after a specific reaction time within 24 h. Continuous formation of nanoparticles was demonstrated by the increasing absorbances of all samples over time. In the meanwhile, the position of the maximum absorbance of each sample did not change significantly, indicating that the chemical composition of nanohybrids at a specific $[\text{Au}^{3+}]/[\text{Ag}^+]$ ratio remained relatively stable over time. The synthesis mechanisms were further analyzed by extracting the data of maximum absorbances between 500 and 600 nm, their positions, and absorbances at 800 nm, and statistically analyzing their potential correlations with metal ions loadings and their mixing ratios. As illustrated in Figure S4a,b, the linearity between the peak position and $[\text{Au}^{3+}]/[\text{Ag}^+]$ ratio was higher than 92%, while the linearity between peak absorbance and Au^{3+} concentration was higher than 93%. At higher Au^{3+} concentrations, i.e., $[\text{Au}^{3+}] \geq 0.63 \text{ mM}$ or $[\text{Au}^{3+}]/[\text{Ag}^+] \geq 0.33:1$, the absorbances deviated from the linear regressions as the ion loadings might exceed the synthesis capacity of LNC and aggregation overrode the formation of individual nanoparticles. As discussed earlier, both LNC aggregation and formation of Ag–AgCl composites could potentially enhance far-red light absorbances.⁶⁹ Hereby, the 800 nm absorbances linearly correlated with Au^{3+} concentration and $[\text{Ag}^+][\text{Cl}^-]$ concentration by over 95 and 89%, respectively, which provided evidence supporting the previous hypotheses. Meanwhile, as the Au^{3+} and Cl^- ions came from the same source, it remains unclear whether Au^{3+} or AgCl was playing the dominant role in far-red light absorbance.

3.3. Antibacterial Activities. Antibacterial activities of the monometallic nanoparticles- and nanohybrids-LNC samples were evaluated against two pathogenic bacterial strains, i.e., *S.*

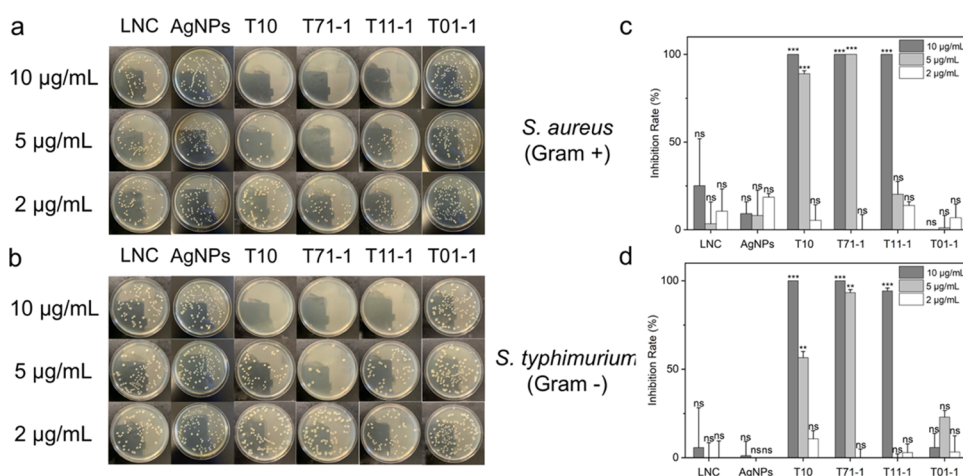


Figure 5. CFU quantification of LNC, and nanoparticles- and nanohybrids-LNC samples at varied concentrations on *S. aureus* and *S. typhimurium*. Agar plate cultures of (a) *S. aureus* and (b) *S. typhimurium* after 24 h treatment with LNC and four samples. Inhibition of (c) *S. aureus* and (d) *S. typhimurium* expressed in percentages of CFU reduction over antibacterial assay using pure sterile water. Significance level of each sample indicated: ***($p < 0.001$), **($p < 0.01$), *($p < 0.05$), and ns ($p > 0.05$, not significant). T71-1 and T11-1 were synthesized by 0.029:1 and 0.20:1 molar ratios of $[\text{Au}^{3+}]/[\text{Ag}^+]$, respectively.

Table 1. Comparison of Silver-based Antibacterial Materials

silver component	carrier	adjuvant	bacterial strain	MIC ($\mu\text{g}/\text{mL}$)	ref
AgNPs	cellulose nanocrystal	polydopamine	<i>B. subtilis</i> (+)	8a	23
			<i>Escherichia coli</i> (−)	4 ^a	
Ag-infused core	lignin nanoparticle	polydiallyldimethyl-ammonium chloride (PDAC)	<i>E. coli</i> (−)	10 ^a	25
			<i>Pseudomonas aeruginosa</i> (−)	77% CFU reduction at 10 ^a	
			<i>Ralstonia sp.</i> (−)	99% CFU reduction at 10 ^a	
AgNPs (spherical and dendritic)	cellulose nanocrystal		<i>S. aureus</i> (+)	4–5 ^a	28
AgNPs	polyphenol (green tea extract)	polyethylene glycol	<i>E. coli</i> (−)	2–3 ^a	
			<i>S. aureus</i> (+)	250	73
			<i>Klebsiella pneumoniae</i> (−)	500	
			<i>E. coli</i> (−)	60	
			<i>P. aeruginosa</i> (−)	125	
			<i>Salmonella enterica</i> (−)	60	
Au-AgNPs			<i>Enterococcus faecalis</i> (+)	2.50 ^a	7
			<i>Pediococcus acidilactici</i> (+)	2.81 ^a	
			<i>E. coli</i> (−)	1.56 ^a	
			<i>P. aeruginosa</i> (−)	1.88 ^a	
Ag/AgCl	reduced graphene oxide	poly(diallyldimethyl-ammonium chloride) (PDDA)	<i>S. aureus</i> (+)	20 (4 ^a)	13
			<i>E. coli</i> (−)	10 (2 ^a)	
Ag/Au/AgCl	LNC		<i>S. aureus</i> (+)	5	this work
			<i>S. typhimurium</i> (−)	10	

^aValues in Ag equivalency, i.e., silver content in the material excluding other elements.

aureus (Gram-positive) and *S. typhimurium* (Gram-negative). The killing power of LNC, T10, T71-1, T11-1, and T01-1 together with a positive AgNPs control (NaBH_4 -AgNPs) was quantitatively determined by CFU reduction compared to the negative control using sterile water at 2, 5, and 10 $\mu\text{g}/\text{mL}$ loadings (Figure 5). On *S. aureus*, T10, T71-1, and T11-1 completely inhibited its bacterial growth at 10 $\mu\text{g}/\text{mL}$, while T01-1 and LNC had no significant inhibitory effect. T71-1 was the only sample that inhibited *S. aureus* growth completely at 5

$\mu\text{g}/\text{mL}$, a significantly low minimum inhibitory concentration (MIC) among AgNPs-based antimicrobial agents (Table 1). In contrast, T10 had an inhibition rate of 88.93% at the same loading, while T11-1 did not inhibit the bacterial growth significantly. NaBH_4 -AgNPs, a classic AgNPs sample, also did not show any significant inhibition at concentrations $\leq 10 \mu\text{g}/\text{mL}$. This comparison corroborated that the antibacterial activity of AgNPs was enhanced when the nanoparticles were in situ synthesized and embedded in the LNC matrix. On *S.*

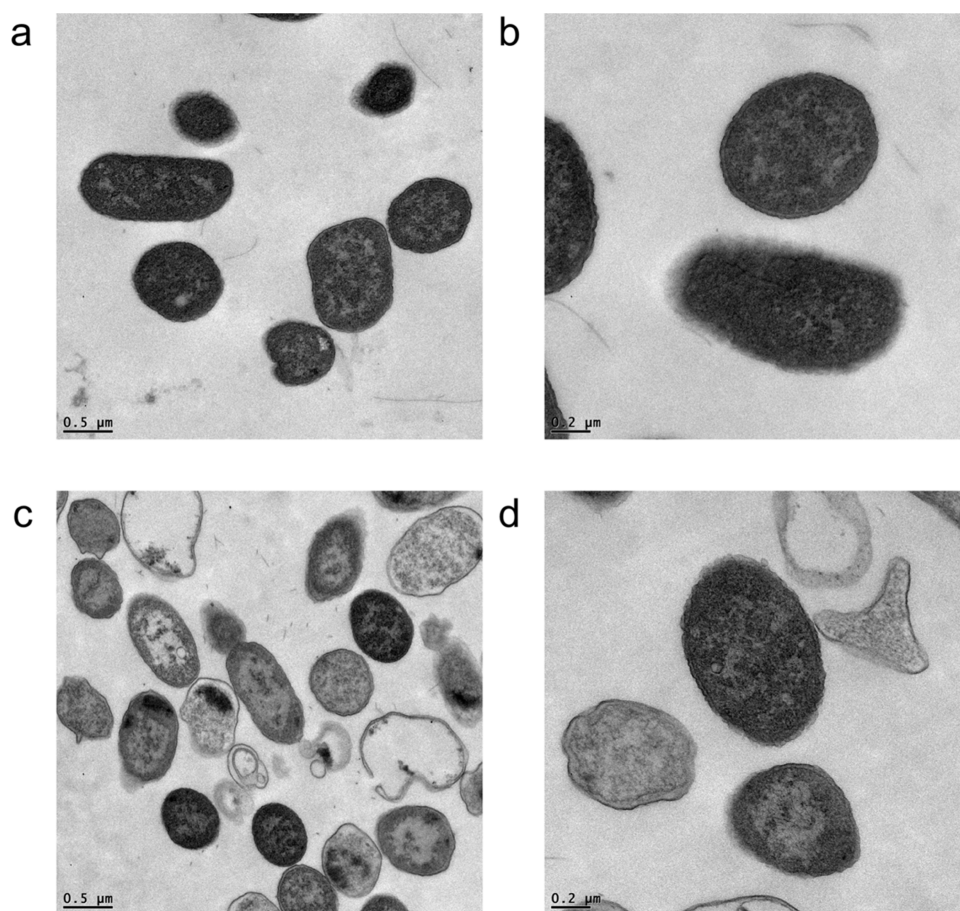


Figure 6. TEM images of (a, b) *S. aureus* and (c, d) *S. typhimurium* cells after 30 min exposure to the nano hybrids-LNC sample T71-1. T71-1 was synthesized by 0.029:1 molar ratio of $[\text{Au}^{3+}]/[\text{Ag}^+]$.

typhimurium, only T10 and T71-1 achieved a full inhibition of bacterial growth at 10 $\mu\text{g}/\text{mL}$, while T11-1 inhibited 94.29% growth at the same loading. At 5 $\mu\text{g}/\text{mL}$, only T10 and T71-1 showed significant inhibition effects by 56.57 and 93.24%, respectively. Across all the loadings, LNC, T01-1, and NaBH_4 -AgNPs did not significantly inhibit bacterial growth of *S. typhimurium* ($p > 0.05$). When the sample loading dropped down to 2 $\mu\text{g}/\text{mL}$, no significant inhibitory effects were observed across all the samples.

To gain a better understanding of the killing mechanism, TEM imaging of *S. aureus* and *S. typhimurium* cell structures after 30 min exposure to a nano hybrids-LNC sample (T71-1) was performed (Figure 6). In the *S. aureus* sample (Figure 6a,b), cell membranes of some cells showed blurred boundaries, implying a disruptive effect of nano hybrids-LNC. In *S. typhimurium*, cell collapse was more noticeable than membrane corruption, as evidenced by morphological changes in the cells. Similar to other silver-based bactericides, rupture of the cell membrane and subsequent leakage of intracellular contents could be one of the mechanisms underlying the antibacterial activities of nano hybrids-LNC.^{7,59,70}

Furthermore, Ag^+ ion release over time was investigated by ICP-OES (Figure S5). To mimic cell culture environment, diluted LB media, same as that used in the antibacterial test, were utilized for dispersing T10, T71-1, and T11-1. Among all three samples, T10 released Ag^+ ions most quickly, reaching 1.61 $\mu\text{g}/\text{mL}$ of Ag^+ within the first hour and tending to level off. Ag^+ release in T71-1 was slower than that in T10 at the

first few hours and then reached a similar level. The coexisting Au and AgCl could be the cause of slower Ag^+ release in T71-1. When more Au and AgCl existed, as in T11-1, Ag^+ release slowed further and only reached 1.07 $\mu\text{g}/\text{mL}$ after 12 h release. Together with the MIC results, the Ag^+ release kinetics clearly indicated the controlled Ag^+ release on antibacterial performances of the nano hybrids. It should be noted that if Ag^+ release was oversuppressed, the antibacterial performances of a nano hybrid would likely be compromised. In comparison to the monometallic T10 and silver-based antibacterial reported in other studies (Table 1), T71-1 was among the most effective, implying an enhanced antibacterial activity potentially due to the coexistence of Ag–Au–AgCl in the nano hybrids. The overall MICs of T71-1 were even lower than the silver equivalency values of many previously reported AgNPs-based products, making it comparably effective at a lower mass concentration and potentially beneficial in commercialization. The environmental effects of nano hybrids-LNC would be much milder as its Ag^+ ion release was highly controlled.^{71,72} The outstanding performance should be attributed to the synergistic effects between the three constituents of the nano hybrid. Although the synergistic mechanism has not been thoroughly revealed, prior research claimed that Ag–Au nanoparticles exhibited increased cell affinity when AuNPs extracted electrons from AgNPs and made the Ag atoms more actively interact with negatively charged bacterial cell membranes.⁷ In addition, Ag–AgCl nano hybrids, also known as a photocatalyst, could generate

ROS under visible light,^{56,58} which could reinforce the ROS induced by Ag⁺ ions and thus enhance the antibacterial activity of the nanohybrids. On the other hand, when the amounts of Au³⁺ and Cl⁻ were increased during synthesis, as in T11-1 versus T71-1, both Ag⁺ ion release and antibacterial activity of the nanohybrids-LNC were significantly reduced, implying that the loading ratio of Ag/Au/AgCl may be a critical factor determining the antibacterial activity of the nanohybrids. Future studies would be needed to elucidate potential synergistic effects of nanohybrid constituents.

4. CONCLUSIONS

Monometallic AgNPs, AuNPs, and Ag–Au–AgCl nanohybrids were successfully synthesized utilizing lignin-containing nanocellulose (LNC) as both reducing and capping agent in one-pot, in situ, chemical-free reactions. The lignin content in LNC and oxygen-containing functional groups played a critical role in Ag⁺ and Au³⁺ ion reduction, while the concentrations and mixing ratios of Ag⁺ and Au³⁺ precursors affected synthesis kinetics and product composition. The nanohybrids-LNC composite exhibited superior antibacterial activities against both Gram-positive and Gram-negative bacterial strains, with low levels of Ag⁺ ions release. This study demonstrated a green route for synthesizing metallic nanoparticles solely with naturally occurring LNC and suggested that coexisting AuNPs and AgCl with AgNPs would enhance antibacterial activities of AgNPs-based bactericides. In future research, the chemistry of LNCs and interactions between AgNPs, AuNPs, and AgCl could be more deeply studied to better understand the mechanisms of nanohybrids synthesis and synergistic antibacterial activities.

■ ASSOCIATED CONTENT

SI Supporting Information

The Supporting Information is available free of charge at <https://pubs.acs.org/doi/10.1021/acsomega.2c05400>.

LNC and BNC preparations; experimental design of nanoparticles and nanohybrids synthesis with LNC and BNC (Tables S1 and S2); UV–vis spectra of BNC samples (Figure S1); XPS whole-range surveys and high-resolution scans of Cl 2p and O 1s regions (Figure S2); UV–vis spectra of nanohybrids-LNC samples with different [Au³⁺]/[Ag⁺] loading ratios over the course of 24 h reaction (Figure S3); linear regressions for nanoparticle synthesis kinetics (Figure S4); Ag⁺ ion release of monometallic AgNPs- (T10) and nanohybrids-LNC (T71-1 and T11-1) samples over time (Figure S5) (PDF)

■ AUTHOR INFORMATION

Corresponding Author

Caixia Wan – Department of Biomedical, Biological, and Chemical Engineering, University of Missouri, Columbia, Missouri 65211, United States; orcid.org/0000-0001-5490-7490; Phone: +1 573 884 7882; Email: wanca@missouri.edu

Authors

Yisheng Sun – Department of Biomedical, Biological, and Chemical Engineering, University of Missouri, Columbia, Missouri 65211, United States

Qianwei Li – Department of Biomedical, Biological, and Chemical Engineering, University of Missouri, Columbia, Missouri 65211, United States

Xiangwei Du – Veterinary Medical Diagnostic Laboratory, College of Veterinary Medicine, University of Missouri, Columbia, Missouri 65211, United States

Velaphi Thipe – Department of Radiology, University of Missouri, Columbia, Missouri 65211, United States

Bongkosh Vardhanabhuti – Division of Food, Nutrition, and Excises Sciences, Columbia, Missouri 65211, United States

Shramik Sengupta – Department of Biomedical, Biological, and Chemical Engineering, University of Missouri, Columbia, Missouri 65211, United States

Kattesh Katti – Department of Radiology, University of Missouri, Columbia, Missouri 65211, United States

Complete contact information is available at:

<https://pubs.acs.org/10.1021/acsomega.2c05400>

Author Contributions

The manuscript was written through the contributions of all of the authors. The authors have given approval to the final version of the manuscript.

Notes

The authors declare no competing financial interest.

■ ACKNOWLEDGMENTS

This work was in part supported by the USDA National Institute of Food and Agriculture (Award No. 2021-67021-34504) and National Science Foundation (Award No. 1933861).

■ REFERENCES

- (1) Rawson, T. M.; Wilson, R. C.; O'Hare, D.; Herrero, P.; Kambugu, A.; Lamorde, M.; Ellington, M.; Georgiou, P.; Cass, A.; Hope, W. W.; Holmes, A. H. Optimizing antimicrobial use: challenges, advances and opportunities. *Nat. Rev. Microbiol.* **2021**, *19*, 747–758.
- (2) Duan, S.; Wu, R.; Xiong, Y.-H.; Ren, H.-M.; Lei, C.; Zhao, Y.-Q.; Zhang, X.-Y.; Xu, F.-J. Multifunctional antimicrobial materials: From rational design to biomedical applications. *Prog. Mater. Sci.* **2022**, *125*, No. 100887.
- (3) Zheng, K.; Setyawati, M. I.; Leong, D. T.; Xie, J. Antimicrobial silver nanomaterials. *Coord. Chem. Rev.* **2018**, *357*, 1–17.
- (4) Zhang, Y.; Ferguson, S. A.; Watanabe, F.; Jones, Y.; Xu, Y.; Biris, A. S.; Hussain, S.; Ali, S. F. Silver Nanoparticles Decrease Body Weight and Locomotor Activity in Adult Male Rats. *Small* **2013**, *9*, 1715–1720.
- (5) Maziero, J. S.; Thipe, V. C.; Rogero, S. O.; Cavalcante, A. K.; Damasceno, K. C.; Ormenio, M. B.; Martini, G. A.; Batista, J. G. S.; Viveiros, W.; Katti, K. K.; et al. Species-Specific in vitro and in vivo Evaluation of Toxicity of Silver Nanoparticles Stabilized with Gum Arabic Protein. *Int. J. Nanomed.* **2020**, *15*, 7359–7376.
- (6) Loza, K.; Heggen, M.; Epple, M. Synthesis, Structure, Properties, and Applications of Bimetallic Nanoparticles of Noble Metals. *Adv. Funct. Mater.* **2020**, *30*, No. 1909260.
- (7) Banerjee, M.; Sharma, S.; Chattopadhyay, A.; Ghosh, S. S. Enhanced antibacterial activity of bimetallic gold-silver core-shell nanoparticles at low silver concentration. *Nanoscale* **2011**, *3*, 5120–5125.
- (8) Haleem, A.; Chen, S.-Q.; Ullah, M.; Siddiq, M.; He, W.-D. Highly porous cryogels loaded with bimetallic nanoparticles as an efficient antimicrobial agent and catalyst for rapid reduction of water-soluble organic contaminants. *J. Environ. Chem. Eng.* **2021**, *9*, No. 106510.

- (9) Nudelman, R.; Gavriely, S.; Bychenko, D.; Barzilay, M.; Gulakhmedova, T.; Gazit, E.; Richter, S. Bio-assisted synthesis of bimetallic nanoparticles featuring antibacterial and photothermal properties for the removal of biofilms. *J. Nanobiotechnol.* **2021**, *19*, 452.
- (10) Shin, Y.; Bae, I.-T.; Arey, B. W.; Exarhos, G. J. Facile Stabilization of Gold-silver Alloy Nanoparticles on Cellulose Nanocrystal. *J. Phys. Chem. C* **2008**, *112*, 4844–4848.
- (11) Lomelí-Marroquín, D.; Medina Cruz, D.; Nieto-Argüello, A.; Vernet Crua, A.; Chen, J.; Torres-Castro, A.; Webster, T. J.; Cholula-Díaz, J. L. Starch-mediated synthesis of mono- and bimetallic silver/gold nanoparticles as antimicrobial and anticancer agents. *Int. J. Nanomed.* **2019**, *14*, 2171–2190.
- (12) Padilla-Cruz, A. L.; Garza-Cervantes, J. A.; Vasto-Anzaldo, X. G.; García-Rivas, G.; León-Buitimea, A.; Morones-Ramírez, J. R. Synthesis and design of Ag–Fe bimetallic nanoparticles as antimicrobial synergistic combination therapies against clinically relevant pathogens. *Sci. Rep.* **2021**, *11*, No. 5351.
- (13) Zhou, Y.; Chen, R.; He, T.; Xu, K.; Du, D.; Zhao, N.; Cheng, X.; Yang, J.; Shi, H.; Lin, Y. Biomedical Potential of Ultrafine Ag/AgCl Nanoparticles Coated on Graphene with Special Reference to Antimicrobial Performances and Burn Wound Healing. *ACS Appl. Mater. Interfaces* **2016**, *8*, 15067–15075.
- (14) Haddar, A.; Ben Ayed, E.; Sila, A.; Putaux, J.-L.; Bougateg, A.; Boufi, S. Hybrid levan–Ag/AgCl nanoparticles produced by UV-irradiation: properties, antibacterial efficiency and application in bioactive poly(vinyl alcohol) films. *RSC Adv.* **2021**, *11*, 38990–39003.
- (15) Dong, Y.-Y.; Deng, F.; Zhao, J.-J.; He, J.; Ma, M.-G.; Xu, F.; Sun, R.-C. Environmentally friendly ultrasound synthesis and antibacterial activity of cellulose/Ag/AgCl hybrids. *Carbohydr. Polym.* **2014**, *99*, 166–172.
- (16) Zhao, M.; Hou, X.; Lv, L.; Wang, Y.; Li, C.; Meng, A. Synthesis of Ag/AgCl modified anhydrous basic bismuth nitrate from BiOCl and the antibacterial activity. *Mater. Sci. Eng. C* **2019**, *98*, 83–88.
- (17) Han, C.; Ge, L.; Chen, C.; Li, Y.; Zhao, Z.; Xiao, X.; Li, Z.; Zhang, J. Site-selected synthesis of novel Ag@AgCl nanoframes with efficient visible light induced photocatalytic activity. *J. Mater. Chem. A* **2014**, *2*, 12594–12600.
- (18) Li, Y.; Ding, Y. Porous AgCl/Ag Nanocomposites with Enhanced Visible Light Photocatalytic Properties. *J. Phys. Chem. C* **2010**, *114*, 3175–3179.
- (19) Zahran, M.; Marei, A. H. Innovative natural polymer metal nanocomposites and their antimicrobial activity. *Int. J. Biol. Macromol.* **2019**, *136*, 586–596.
- (20) Moon, R. J.; Martini, A.; Nairn, J.; Simonsen, J.; Youngblood, J. Cellulose nanomaterials review: structure, properties and nanocomposites. *Chem. Soc. Rev.* **2011**, *40*, 3941–3994.
- (21) Wege, H. A.; Kim, S.; Paunov, V. N.; Zhong, Q.; Velev, O. D. Long-Term Stabilization of Foams and Emulsions with In-Situ Formed Microparticles from Hydrophobic Cellulose. *Langmuir* **2008**, *24*, 9245–9253.
- (22) Frangville, C.; Rutkevicius, M.; Richter, A. P.; Velev, O. D.; Stoyanov, S. D.; Paunov, V. N. Fabrication of Environmentally Biodegradable Lignin Nanoparticles. *ChemPhysChem* **2012**, *13*, 4235–4243.
- (23) Shi, Z.; Tang, J.; Chen, L.; Yan, C.; Tanvir, S.; Anderson, W. A.; Berry, R. M.; Tam, K. C. Enhanced colloidal stability and antibacterial performance of silver nanoparticles/cellulose nanocrystal hybrids. *J. Mater. Chem. B* **2015**, *3*, 603–611.
- (24) Kaushik, M.; Li, A. Y.; Hudson, R.; Masnadi, M.; Li, C.-J.; Moores, A. Reversing aggregation: direct synthesis of nanocatalysts from bulk metal. Cellulose nanocrystals as active support to access efficient hydrogenation silver nanocatalysts. *Green Chem.* **2016**, *18*, 129–133.
- (25) Richter, A. P.; Brown, J. S.; Bharti, B.; Wang, A.; Gangwal, S.; Houck, K.; Hubal, E. A. C.; Paunov, V. N.; Stoyanov, S. D.; Velev, O. D. An environmentally benign antimicrobial nanoparticle based on a silver-infused lignin core. *Nat. Nanotechnol.* **2015**, *10*, 817–823.
- (26) Lintinen, K.; Luiro, S.; Figueiredo, P.; Sakarinen, E.; Mousavi, Z.; Seitsonen, J.; Rivièrè, G. N. S.; Mattinen, U.; Niemelä, M.; Tammela, P.; et al. Antimicrobial Colloidal Silver–Lignin Particles via Ion and Solvent Exchange. *ACS Sustainable Chem. Eng.* **2019**, *7*, 15297–15303.
- (27) Rak, M. J.; Friščić, T.; Moores, A. One-step, solvent-free mechanosynthesis of silver nanoparticle-infused lignin composites for use as highly active multidrug resistant antibacterial filters. *RSC Adv.* **2016**, *6*, 58365–58370.
- (28) Xiong, R.; Lu, C.; Zhang, W.; Zhou, Z.; Zhang, X. Facile synthesis of tunable silver nanostructures for antibacterial application using cellulose nanocrystals. *Carbohydr. Polym.* **2013**, *95*, 214–219.
- (29) Ifuku, S.; Tsuji, M.; Morimoto, M.; Saimoto, H.; Yano, H. Synthesis of Silver Nanoparticles Templated by TEMPO-Mediated Oxidized Bacterial Cellulose Nanofibers. *Biomacromolecules* **2009**, *10*, 2714–2717.
- (30) She, Q.; Li, J.; Lu, Y.; Lin, S.; You, R. In situ synthesis of silver nanoparticles on dialdehyde cellulose as reliable SERS substrate. *Cellulose* **2021**, *28*, 10827–10840.
- (31) Chen, S.; Wang, G.; Sui, W.; Parvez, A. M.; Si, C. Synthesis of lignin-functionalized phenolic nanosphere supported Ag nanoparticles with excellent dispersion stability and catalytic performance. *Green Chem.* **2020**, *22*, 2879–2888.
- (32) Islam, M. S.; Akter, N.; Rahman, M. M.; Shi, C.; Islam, M. T.; Zeng, H.; Azam, M. S. Mussel-Inspired Immobilization of Silver Nanoparticles toward Antimicrobial Cellulose Paper. *ACS Sustainable Chem. Eng.* **2018**, *6*, 9178–9188.
- (33) Pawcenis, D.; Chlebda, D. K.; Jędrzejczyk, R. J.; Leśniak, M.; Sitarz, M.; Łojewska, J. Preparation of silver nanoparticles using different fractions of TEMPO-oxidized nanocellulose. *Eur. Polym. J.* **2019**, *116*, 242–255.
- (34) Jia, X.; Yao, Y.; Yu, G.; Qu, L.; Li, T.; Li, Z.; Xu, C. Synthesis of gold-silver nanoalloys under microwave-assisted irradiation by deposition of silver on gold nanoclusters/triple helix glucan and antifungal activity. *Carbohydr. Polym.* **2020**, *238*, No. 116169.
- (35) Landge, V. K.; Sonawane, S. H.; Manickam, S.; Bhaskar Babu, G. U.; Boczkaj, G. Ultrasound-assisted wet-impregnation of Ag–Co nanoparticles on cellulose nanofibers: Enhanced catalytic hydrogenation of 4-nitrophenol. *J. Environ. Chem. Eng.* **2021**, *9*, No. 105719.
- (36) Ahmed, H. B.; Attia, M. A.; El-Dars, F. M. S. E.; Emam, H. E. Hydroxyethyl cellulose for spontaneous synthesis of antipathogenic nanostructures: (Ag & Au) nanoparticles versus Ag-Au nano-alloy. *Int. J. Biol. Macromol.* **2019**, *128*, 214–229.
- (37) Chandna, S.; Thakur, N. S.; Reddy, Y. N.; Kaur, R.; Bhaumik, J. Engineering Lignin Stabilized Bimetallic Nanocomplexes: Structure, Mechanistic Elucidation, Antioxidant, and Antimicrobial Potential. *ACS Biomater. Sci. Eng.* **2019**, *5*, 3212–3227.
- (38) Yang, W.; Fortunati, E.; Gao, D.; Balestra, G. M.; Giovane, G.; He, X.; Torre, L.; Kenny, J. M.; Puglia, D. Valorization of Acid Isolated High Yield Lignin Nanoparticles as Innovative Antioxidant/Antimicrobial Organic Materials. *ACS Sustainable Chem. Eng.* **2018**, *6*, 3502–3514.
- (39) Hu, X.; Xu, X.; Fu, F.; Yang, B.; Zhang, J.; Zhang, Y.; Touhid, S. S.; Liu, L.; Dong, Y.; Liu, X.; Yao, J. Synthesis of bimetallic silver-gold nanoparticle composites using a cellulose dope: Tunable nanostructure and its biological activity. *Carbohydr. Polym.* **2020**, *248*, No. 116777.
- (40) Solala, I.; Iglesias, M. C.; Peresin, M. S. On the potential of lignin-containing cellulose nanofibrils (LCNFs): a review on properties and applications. *Cellulose* **2020**, *27*, 1853–1877.
- (41) Spieser, H.; Denneulin, A.; Deganello, D.; Gethin, D.; Koppolu, R.; Bras, J. Cellulose nanofibrils and silver nanowires active coatings for the development of antibacterial packaging surfaces. *Carbohydr. Polym.* **2020**, *240*, No. 116305.
- (42) Dong, H.; Snyder, J. F.; Tran, D. T.; Leadore, J. L. Hydrogel, aerogel and film of cellulose nanofibrils functionalized with silver nanoparticles. *Carbohydr. Polym.* **2013**, *95*, 760–767.
- (43) Sirviö, J. A.; Ismail, M. Y.; Zhang, K.; Tejesvi, M. V.; Ämmälä, A. Transparent lignin-containing wood nanofiber films with UV-

- blocking, oxygen barrier, and anti-microbial properties. *J. Mater. Chem. A* **2020**, *8*, 7935–7946.
- (44) Nair, S. S.; Chen, H.; Peng, Y.; Huang, Y.; Yan, N. Poly(lactic Acid) Biocomposites Reinforced with Nanocellulose Fibrils with High Lignin Content for Improved Mechanical, Thermal, and Barrier Properties. *ACS Sustainable Chem. Eng.* **2018**, *6*, 10058–10068.
- (45) Hu, S.; Hsieh, Y.-L. Synthesis of surface bound silver nanoparticles on cellulose fibers using lignin as multi-functional agent. *Carbohydr. Polym.* **2015**, *131*, 134–141.
- (46) Murray, C. J.; Ikuta, K. S.; Sharara, F.; Swetschinski, L.; Robles Aguilar, G.; Gray, A.; Han, C.; Bisignano, C.; Rao, P.; Wool, E.; et al. Global burden of bacterial antimicrobial resistance in 2019: a systematic analysis. *Lancet* **2022**, *399*, 629–655.
- (47) Laxminarayan, R. The overlooked pandemic of antimicrobial resistance. *Lancet* **2022**, *399*, 606–607.
- (48) Mavani, K.; Shah, M. Synthesis of silver nanoparticles by using sodium borohydride as a reducing agent. *Int. J. Eng. Res. Technol.* **2013**, *2*, 1–5.
- (49) Sluiter, A.; Hames, B.; Ruiz, R.; Scarlata, C.; Sluiter, J.; Templeton, D.; Crocker, D. Determination of structural carbohydrates and lignin in biomass. *Lab. Anal. Proced.* **2008**, 1–16.
- (50) Li, Y.; Fu, Q.; Yu, S.; Yan, M.; Berglund, L. Optically Transparent Wood from a Nanoporous Cellulosic Template: Combining Functional and Structural Performance. *Biomacromolecules* **2016**, *17*, 1358–1364.
- (51) Sarina, S.; Waclawik, E. R.; Zhu, H. Photocatalysis on supported gold and silver nanoparticles under ultraviolet and visible light irradiation. *Green Chem.* **2013**, *15*, 1814–1833.
- (52) Linic, S.; Christopher, P.; Ingram, D. B. Plasmonic-metal nanostructures for efficient conversion of solar to chemical energy. *Nat. Mater.* **2011**, *10*, 911–921.
- (53) Eustis, S.; El-Sayed, M. A. Why gold nanoparticles are more precious than pretty gold: Noble metal surface plasmon resonance and its enhancement of the radiative and nonradiative properties of nanocrystals of different shapes. *Chem. Soc. Rev.* **2006**, *35*, 209–217.
- (54) Zakaria, H. M.; Shah, A.; Konieczny, M.; Hoffmann, J. A.; Nijdam, A. J.; Reeves, M. E. Small Molecule- and Amino Acid-Induced Aggregation of Gold Nanoparticles. *Langmuir* **2013**, *29*, 7661–7673.
- (55) Ezra, L.; O'Dell, Z. J.; Hui, J.; Riley, K. R. Emerging investigator series: quantifying silver nanoparticle aggregation kinetics in real-time using particle impact voltammetry coupled with UV–vis spectroscopy. *Environ. Sci.: Nano* **2020**, *7*, 2509–2521.
- (56) Chen, D.; Li, T.; Chen, Q.; Gao, J.; Fan, B.; Li, J.; Li, X.; Zhang, R.; Sun, J.; Gao, L. Hierarchically plasmonic photocatalysts of Ag/AgCl nanocrystals coupled with single-crystalline WO₃ nanoplates. *Nanoscale* **2012**, *4*, 5431–5439.
- (57) Liu, C.; Yang, D.; Wang, Y.; Shi, J.; Jiang, Z. Fabrication of antimicrobial bacterial cellulose–Ag/AgCl nanocomposite using bacteria as versatile biofactory. *J. Nanopart. Res.* **2012**, *14*, 1084.
- (58) Wang, P.; Huang, B.; Qin, X.; Zhang, X.; Dai, Y.; Wei, J.; Whangbo, M.-H. Ag@AgCl: A Highly Efficient and Stable Photocatalyst Active under Visible Light. *Angew. Chem., Int. Ed.* **2008**, *47*, 7931–7933.
- (59) Panicker, S.; Ahmady, I. M.; Han, C.; Chehimi, M.; Mohamed, A. A. On demand release of ionic silver from gold-silver alloy nanoparticles: fundamental antibacterial mechanisms study. *Mater. Today Chem.* **2020**, *16*, No. 100237.
- (60) Safavi, A.; Ahmadi, R.; Mohammadpour, Z. Colorimetric sensing of silver ion based on anti aggregation of gold nanoparticles. *Sens. Actuators, B* **2017**, *242*, 609–615.
- (61) Hoflund, G. B.; Hazos, Z. F.; Salaita, G. N. Surface characterization study of Ag, AgO, and Ag₂O using x-ray photoelectron spectroscopy and electron energy-loss spectroscopy. *Phys. Rev. B* **2000**, *62*, 11126–11133.
- (62) Wang, J.; An, C.; Zhang, M.; Qin, C.; Ming, X.; Zhang, Q. Photochemical conversion of AgCl nanocubes to hybrid AgCl–Ag nanoparticles with high activity and long-term stability towards photocatalytic degradation of organic dyes. *Can. J. Chem.* **2012**, *90*, 858–864.
- (63) Chimentão, R.; Cota, I.; Dafinov, A.; Medina, F.; Sueiras, J. E.; Gómez de la Fuente, J. L.; Fierro, J. L. G.; Cesteros, Y.; Salagre, P. Synthesis of silver-gold alloy nanoparticles by a phase-transfer system. *J. Mater. Res.* **2006**, *21*, 105–111.
- (64) Database, N. X. r. P. S. NIST Standard Reference Database Number 20; National Institute of Standards and Technology: Gaithersburg MD, 2000; Vol. 20899.
- (65) Suh, I.-K.; Ohta, H.; Waseda, Y. High-temperature thermal expansion of six metallic elements measured by dilatation method and X-ray diffraction. *J. Mater. Sci.* **1988**, *23*, 757–760.
- (66) Hull, S.; Keen, D. A. Pressure-induced phase transitions in AgCl, AgBr, and AgI. *Phys. Rev. B* **1999**, *59*, 750–761.
- (67) Liu, H.; Song, J.; Shang, S.; Wang, D. Cellulose Nanocrystal/Silver Nanoparticle Composites as Bifunctional Nanofillers within Waterborne Polyurethane. *ACS Appl. Mater. Interfaces* **2012**, *4*, 2413–2419.
- (68) Hasan, A.; Waibhaw, G.; Saxena, V.; Pandey, L. M. Nanobiocomposite scaffolds of chitosan, carboxymethyl cellulose and silver nanoparticle modified cellulose nanowhiskers for bone tissue engineering applications. *Int. J. Biol. Macromol.* **2018**, *111*, 923–934.
- (69) Rocha, F. S.; Gomes, A. J.; Lunardi, C. N.; Kaliaguine, S.; Patience, G. S. Experimental methods in chemical engineering: Ultraviolet visible spectroscopy–UV-Vis. *Can. J. Chem. Eng.* **2018**, *96*, 2512–2517.
- (70) Yin, I. X.; Zhang, J.; Zhao, I. S.; Mei, M. L.; Li, Q.; Chu, C. H. The Antibacterial Mechanism of Silver Nanoparticles and Its Application in Dentistry. *Int. J. Nanomed.* **2020**, *15*, 2555–2562.
- (71) Nicholas, T. P.; Kavanagh, T. J.; Faustman, E. M.; Altemeier, W. A. The Effects of Gene × Environment Interactions on Silver Nanoparticle Toxicity in the Respiratory System. *Chem. Res. Toxicol.* **2019**, *32*, 952–968.
- (72) Zhang, J. L.; Zhou, Z. P.; Pei, Y.; Xiang, Q. Q.; Chang, X. X.; Ling, J.; Shea, D.; Chen, L. Q. Metabolic profiling of silver nanoparticle toxicity in *Microcystis aeruginosa*. *Environ. Sci.: Nano* **2018**, *5*, 2519–2530.
- (73) Rolim, W. R.; Pelegrino, M. T.; de Araújo Lima, B.; Ferraz, L. S.; Costa, F. N.; Bernardes, J. S.; Rodrigues, T.; Brocchi, M.; Seabra, A. B. Green tea extract mediated biogenic synthesis of silver nanoparticles: Characterization, cytotoxicity evaluation and antibacterial activity. *Appl. Surf. Sci.* **2019**, *463*, 66–74.